Twenty-Seventh Symposium (International) on Combustion/The Combustion Institute, 1998/pp. 659–666

WRINKLING, POCKET FORMATION, AND DOUBLE PREMIXED FLAME INTERACTION PROCESSES

PAUL-HENRI RENARD, JUAN CARLOS ROLON, DOMINIQUE THÉVENIN AND SÉBASTIEN CANDEL

Laboratoire E.M2.C.
École Centrale Paris et CNRS
Grande Voie des Vignes
F-92295 Châtenay-Malabry, France

An experimental method of investigation is used to analyze some fundamental features of a double laminar premixed flame interacting with a single vortex ring. A steady double premixed counterflow flame of propane and air is first established between two opposed nozzles. A vortex ring is generated from a cylindrical tube installed in the lower combustor nozzle and impinges on one flame if the vortex is weak and on both flames if not. The interaction between the toroidal vortex and the lower flame provides complementary information on the fundamental interaction processes previously studied by Driscoll and coworkers. Comparisons with the numerical simulations of Poinsot et al. are made and confirm the theoretical predictions. The interaction between the vortex and the upper reactive layer is also interesting as it gives information on the dynamics of two colliding premixed flames and can be used to investigate flamefront mutual interaction processes. The ability of the vortex to reach the second flame front is characterized by a new number $Tr(r)$, and flame merging processes are discussed.

Introduction

The interaction between flames and vortices has fundamental and practical implications. This problem is examined, for instance, to characterize different regimes of turbulent combustion. Diagrams distinguishing the various modes of combustion were first constructed on intuitive, theoretical, and dimensional considerations [1–3]. More recent studies relied on direct numerical simulations (DNSs) of flame/vortex interactions [4,5]. Because turbulent combustion often features thin reactive layers evolving in a field of multiscale eddies, the flame/vortex problem typifies elementary interaction processes controlling the burning rate.

Previous studies carried out in the field of premixed flame/vortex interactions only concerned a single vortex ring (or a single vortex pair in a two-dimensional configuration) and a single flame. Poinsot et al. [4] revised the classification made by Peters [3] using DNS calculations. It was concluded that the flamelet concept was valid in a domain much larger than that predicted by the standard combustion diagram [3]. In particular, the Klimov–Williams criterion was found to be inadequate, the Kolmogorov vortices being unable to strongly affect the flame front because of their small size and their short lifetime.

Experimental investigations are not easy to perform and are therefore less numerous. They are of three kinds. The first one concerns the interaction of an upwardly propagating, laminar premixed flame with a vortex ring traveling downward. This configuration was extensively explored by Driscoll and coworkers [6–10]. They confirmed the conclusions reached by Poinsot et al. [4] but could not investigate all the spectral diagram as they only managed to scan the domain of large vortices ($r/\delta_f > 10$). Another configuration corresponds to the interaction of a branch of a V-shaped premixed flame with a Kàrmàn vortex street. It was investigated in a series of other studies [11–16]. More recently, Nguyen and Paul examined the interaction between a two-dimensional vortex with a V-shaped flame [17]. For these last two cases, the configuration is more complex, making the interpretation more difficult.

A justification for studying double flame interactions is that visualizations of realistic flame fronts show corrugated structures in many practical situations. It results in several coexisting flame fronts that interact altogether. Using this fact, François et al. [18] studied the interaction between two premixed laminar V-shaped flame fronts to investigate flame front cancellation. They observed a repulsion between the two oblique flame fronts separated by fresh gases.

This paper describes experimental results on a novel configuration in which a vortex ring interacts with a double premixed counterflow flame. This geometry extends our previous work on the interaction between a strained non-premixed flame and a vortex [19–21]. This is a particularly interesting geometry, allowing investigations of flame/vortex interactions

for much smaller vortices than those studied in previous papers [6–10]. In addition, interactions between colliding flame fronts can be examined. Using time-resolved visualization (spontaneous emission on OH and CH radicals), the dynamics of the flame is analyzed when interacting with the vortex ring. The experimental setup is first briefly described. The second section details the operating conditions. Some typical results are then described in the third section, and the spectral diagram is analyzed. Finally, two cases of double flame interactions are considered and discussed.

Experimental Setup

The apparatus consists of a counterflow burner and an intensified charge-coupled device (ICCD) camera. The burner comprises two opposite identical nozzles between which two premixed flames are stabilized symmetrically on both sides of the stagnation plane. These two flames are submitted to the same constant strain rate, which may be varied by changing the injection flowrates of the reactants or the distance between the two nozzles. The main advantage of this configuration lies in the flames being almost flat and well stabilized in the flow and the separation distance between them being easily controllable.

Each injection nozzle has a 20-mm diameter and is surrounded by an annular nozzle with an outer diameter of 39 mm. The reactant mixture is injected through the central nozzle while the outer sheet of nitrogen insulates the reactive stream from external disturbances. The distance between the nozzle outlet planes b is set to 40 mm throughout this study. Both nozzles are fed with a mixture of propane and air at ambient temperature and pressure. It is worth defining the equivalence ratio as $\phi = (\dot{m}_f/\dot{m}_o)/(\dot{m}_f/\dot{m}_o)_{st}$ where $\dot{m}_f$ and $\dot{m}_o$ are the mass flow rates of fuel and oxidizer (here, air) and subscript st refers to their stoichiometric values. This quantity is swept in the 0.5 to 1.1 range. Richer flames are not studied because of burner overheating. However, if we restrict our study to stabilizing thermodiffusion cases, there should be no need for richer flames as the whole range of laminar burning velocities is covered, with the maximum being reached at $\phi \approx 1.1$.

Along the axis of the lower nozzle, a cylindrical tube with an internal diameter $d = 2$ mm is connected to a cylindrical plenum chamber (diameter $D = 25$ mm) and generates a single laminar vortex ring through the displacement of a volume v_G of mixture by a piston located in this chamber. The actuator, which moves the piston, is excited by a voltage ramp with a rise time τ_r. A more extensive description of this device, initially used in a non-premixed configuration, is given in Ref. [19]. In this study, τ_r is kept constant to 10 ms while v_G is varied ($v_G = 50 - 900$ mm^3) to get various vortex strengths.

We focus on both OH ($A^2\Sigma^+ - X^2\Pi$) and CH ($A^2\Delta - X^2\Pi$) transitions. Dandy and Vosen [22] showed that OH chemiluminescence is an exponential function of the equivalence ratio, and consequently a sensitive tracer of the reaction intensity. Moreover, CH spontaneous emission is widely regarded as a good tracer of the reaction zone [23], even if its role in reaction processes is not completely understood [24,25]. Single-shot images of the region between both nozzles are made using an ICCD camera that collects the chemiluminescence signal:

- Between 305 and 320 nm by means of a WG-305 highpass filter and a UG-5 bandpass filter for OH radicals
- Between 425 and 435 nm by means of a bandpass filter (50% cutoff wavelength at 428 and 434 nm) filter for CH radicals

In this way, the chemiluminescence emitted by the Q (0,0) and Q (1,1) vibrational bands of OH (respectively the Q (0,0) and Q (2,2) vibrational bands of CH) is isolated and integrated during the exposure time (chosen sufficiently short to neglect the effect of gas motion). The magnitude of the spontaneous fluorescence signal is much lower than that corresponding to chemiluminescence so that the images are not confused by the presence of OH in hot gases.

Experiments were conducted as follows. A steady double flame is first stabilized. At a selected instant t_0, a toroidal vortex is impulsively injected by the movement of the piston. The vortex ring progresses toward the flame. At a well-defined instant $t_1 \geq t_0$, the shutter of the ICCD camera is opened during a short exposure time. As the experiment is perfectly reproducible, one can get the whole time sequence of the interaction by choosing different instants t_1. The reaction zone structure is monitored by imaging both OH and CH chemiluminescence during the interaction with the vortex ring. As the signal of a large number of spectral lines is collected to visualize the flame front, it cannot be assumed that the initial rovibrational level population is insensitive to temperature variations. It is therefore impossible to get quantitative information on the concentration of OH and CH species. Nevertheless, the data provide the shape of the flame front as it interacts with the vortex.

Operating Conditions

Our experimental setup is fundamentally different from the configuration of Ref. [6] for at least two reasons: (1) the flame is initially flat and strained in a counterflow instead of being curved and unstrained in a duct; and (2) heat losses are low (about 20 K) in the experiment of Ref. [6], whereas they are somewhat higher in our configuration. *Heat*

TABLE 1
Comparison between theory (full chemistry simulation) and experiment (thermocouple measurements). T_{ad} is the adiabatic temperature predicted by the simulation. T_{sp} is the stagnation point temperature measured in the experiment. The reduced temperature Θ is also calculated and can be compared with 0.55, which is the typical value for Poinsot et al. simulations.

ϕ	0.6	0.7	0.8	0.9	1.0	1.1
T_{ad}(K)	—	1830	2000	2120	2230	—
T_{sp}(K)	1450	1650	1800	1900	1950	1900
Θ	—	0.88	0.88	0.88	0.85	—

losses must be interpreted in their broadest sense as any mechanism that can cause a decrease of temperature by convection, conduction, or radiation. Previous measurements of temperature for the same burner indicated that the temperature at the stagnation point is about 200 K lower than the adiabatic flame temperature (see Table 1) [26,27]. The measurements were achieved by a Pt-Rd/Pt thermocouple with a radiation correction, and the simulations were made with a one-dimensional code using detailed chemistry and complex transport. It gives an order of magnitude of heat losses, mainly due to counterflow stretch in this configuration (i.e., heat losses driven by convection). Bearing in mind that their effect is mainly sensitive on flame extinction, quenching the flame should be made quite easier (because of nonnegligible heat losses). In the same way, it is known from previous work that thermodiffusive instabilities can locally lower temperature. For instance, in cellular structures, the flame appears darker at the crests of the cells than at its troughs and sometimes disappears entirely, indicating that the temperature at the crests is lower than in other parts of the cells [28,29]. Thus, thermodiffusive effects may contribute to flame extinction, but this mechanism may be not sufficient. But we study here propane/air flames with a Lewis number, *Le*, greater than one, so thermodiffusion tends to make extinction more difficult.

To build a spectral diagram, we first need to define some fundamental quantities. The classical analysis of Zeldovitch, Frank-Kamenetskii, and Semenov (1938) permits derivation of an expression for the flame thickness δ_f: $\delta_f \sim 7.4\ (\lambda/c_p)_{T_{ref}}/(\rho_u S_L)$, where λ and c_p are typical values of the thermal conductivity and the specific heat of the unburnt gas mixture at a reference temperature (here $T_{ref} = 300$ K), ρ_u is the density of the unburnt gases, and S_L is the laminar burning velocity [6]. It must be noticed that this formula refers to an unstretched flame. Knowing that the initial stretch induced by the counterflow (which is always lower than 50 s^{-1}) is only aimed at stabilizing the double flame and considering, for instance, the experimental results of Wu and Law [30], the burning velocity varies very little in our experiment for a wide range of counterflow strain rates. The slight errors on δ_f and S_L induced by this approximation do not matter, as the spectral diagram only gives information on orders of magnitude. In the same way, the limits of the different regimes are not affected by the reactant mass flux as the definition of *no effect, wrinkled flame, pocket formation,* and *quenching* regions is phenomenological. The laminar burning velocity S_L for a mixture of C_3H_8 and air is determined from previous works [30–32].

Another difference between the premixed flame/vortex interactions studied here and those of Roberts and Driscoll is that the toroidal vortex is small enough so that the flame dynamics cannot be likened to that of a counterflow flame produced between a stream of cold reactants and an opposing stream of hot products [8]. In our configuration, curvature effects are not negligible, and, thus, it complements these previous studies. We can investigate other spectral regions calculated by Poinsot et al. but for which no experimental results were available yet.

Concerning the vortex ring, velocity measurements [19] indicate that the diameter of the vortex ring is about equal to the diameter d of the generator. Assuming that the core corresponds to the region of solid body rotation, it was found that the core diameter is nearly equal to $3d/4$. The Reynolds number, *Re*, of the vortex is defined as $Re = (u_\theta d)/\nu$ where u_θ is the azimuthal velocity of the vortex, d is the diameter of the vortex generator (as the diameter of the ring is almost the same), and ν is the kinematic viscosity of fresh gases. In our experiments, the *Re* was varied between 70 and 1400. The translational speed U_T of the vortex ring in the laboratory reference frame is of the same order as u_θ [6].

Examples of Interactions

Typical features of single flame/vortex interactions are first discussed. The two flames are stabilized in the counterflow in such a way to be as far apart from each other as possible.

Flame Wrinkling ($\phi = 0.7$, $Re = 440$)

We first consider a case where the vortex pair size ($d/\delta_f = 3.63$) and speed ($u_\theta/S_L = 7.3$) are sufficiently large to wrinkle the flame but not large enough to induce pocket formation. Fig. 1 displays the spontaneous emission of CH radicals at $t = 5$ ms after the vortex ring begins to impinge on the flame. The time t, when normalized by the characteristic chemical time of the flame δ_f/S_L, is $t^+ = 2.7$. It is not easy to properly determine the end of the interaction, because the flame needs a very long time to

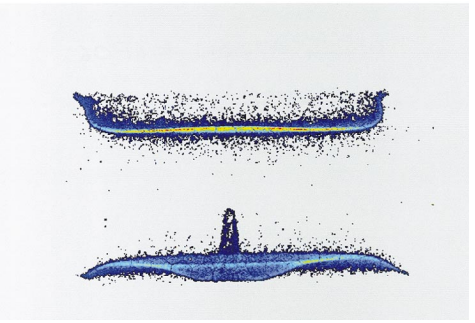

FIG. 1. Wrinkled flame (CH spontaneous emission, $\phi = 0.7$, $Re = 440$, $u_\theta/S_L = 7.3$, $d/\delta_f = 3.63$).

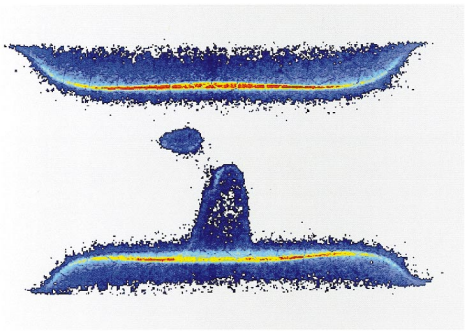

FIG. 2. Formation of a pocket (OH spontaneous emission, $\phi = 0.5$, $Re = 600$, $u_\theta/S_L = 44.1$, $d/\delta_f = 0.83$).

recover its initial shape. So we define the interaction time as the interval between the vortex/flame collision and the instant when the flame starts to move back to the lower burner. With this definition, one may conclude that the interaction time is 2.9 chemical times. The vortex, after having crossed the second flame, enters the upper nozzle and perturbs the flow. This configuration belongs to the regime of wrinkled flame sheets.

Pocket Formation ($\phi = 0.5$, $Re = 600$)

Pinching of the flame front appears when increasing the vortex speed. It later induces the formation of pockets of fresh gases in the burnt gas region. Fig. 2 shows the OH spontaneous emission for a typical case ($u_\theta/S_L = 44.1$, $d/\phi_f = 0.83$) 6 ms after the beginning of the interaction. It corresponds to $t^+ = 0.17$. This configuration belongs to the regime of corrugated flame sheets. The pocket of fresh gases is surrounded by a reactive layer, but it is not easy to determine whether this flame front is quenched. The experimental results indicate that the life duration of all the pockets we observed was lower than 1 ms. Unfortunately, the mechanisms implied in the formation of these pockets are very complex, and this difficulty is reinforced by the counterflow: when the pocket is formed, it is very rare that it evolves symmetrically; it is therefore shifted sideways in the counterflow and rapidly convected far away (see Fig. 2). Hence, it is difficult to produce the same pocket several times to track the time evolution of the flame front around it. Besides, OH and CH spontaneous emission do not provide images with sufficient signal to detect an extinction. Planar laser-induced fluorescence (PLIF) on OH and CH radicals would be more appropriate with the restrictions that hot gases would perturb the OH PLIF imaging while CH is not clearly proved to be a good marker of the extinction.

Turbulent Vortex/Flame Interaction ($\phi = 0.9$, $Re = 1380$)

When the strength of the vortex is increased, instabilities appear: the vortex becomes *turbulent*. It does not mean that the flow inside the vortex is turbulent, but the ring structure is no more regular because of instabilities that recall turbulence behavior. This makes the interpretation of flame/vortex interaction problematic. Formations of pockets are still visible (very often, several small pockets are formed), but the structure of the flame front is too complicated to give valuable information for a combustion diagram. As the vortex is moving further into hot gases (between both flames), instabilities tend to disappear. The viscosity, at least 10 times higher in hot gases than in the unburnt ones, dissipates very quickly a large amount of the vorticity of the toroidal vortex, which then recovers a laminar behavior. Later on, it leads back to a smooth flame structure (see Fig. 4).

This limitation of our present experimental setup makes flame quenching unlikely. Heat losses in the simulations of Poinsot et al. [4] are very high, to ensure local extinction of the flame: if T_u (respectively T_b) denotes the temperature of unburnt (respectively adiabatic flame burnt) gases, then the reduced temperature $\Theta = (T - T_u)/(T_b - T_u)$ typically reaches a maximum of 0.95 in the reaction zone and falls down to 0.55 at the downstream numerical boundary [4]. Moreover, the Lewis number of their simulations is close to 1 (0.8 and 1.2). Thus, in the less-conducive case to quenching, thermodiffusive effects just stabilize the flame front a little. In our experiments, propane is used and its Lewis number is always larger than 1. The nondimensional temperature Θ is about 0.9, indicating much lower heat losses (see Table 1). All this renders the investigation of the quenching limit difficult in our experiment, contrary to Poinsot's simulations.

Spectral Diagram

In the previous section, we mentioned that there are four well-known kinds of premixed flame/vortex

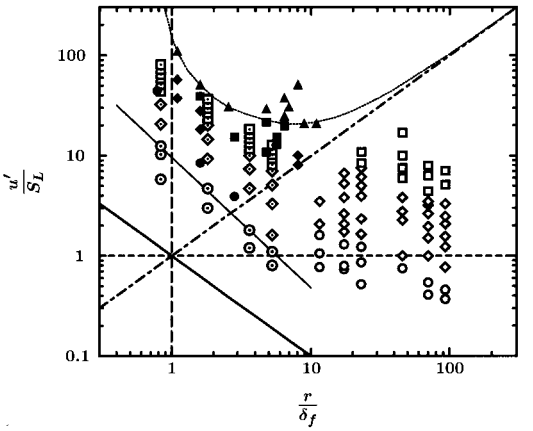

FIG. 3. Single vortex quenching curve. Hollow symbols correspond to a propane flame, $\phi = 0.6$, $Le = 1.87$, $S_L = 14$ cm s^{-1}, $\delta_f = 0.55$ mm (Roberts and Driscoll [6]). Dotted hollow symbols are our measurements for different values of ϕ. Filled symbols are the simulations of Poinsot et al. [4]. Circles correspond to the no-effect region, diamonds to the wrinkled flame region, squares to the pocket formation region, and triangles to the quenching region. The solid line is the Kolmogorov line ($Re = 1$). The dashed line represents $Vr(r) = 1$. The long-dashed line corresponds to $P(r) = 1$. The dashed-dotted line is the line $Ka = 1$. The dotted line is the quenching limit deduced from DNS calculations of Poinsot et al. The thin solid line is the no-effect limit coming from our measurements.

interactions (three were experimentally observed in this study). Poinsot et al. explain how to exploit these results [4,5]. The multiple-scale nature of the interaction between the flame and the flowfield implies that a spectral diagram may be built for each point of the combustion diagram. This diagram ranges from the integral scale (l, u'_{RMS}) of the flow to the Kolmogorov scale (η, u'_K). Results from Roberts et al. and Poinsot et al. are summarized in Fig. 3. We use the same assumptions and the spectral diagram layout as in Refs. [4,5]: the coordinates are r/δ_f and u'/S_L, where r and u' denote the characteristic length and velocity scales of the eddy and δ_f and S_L refer to the unstretched flame thickness and laminar burning velocity. These four parameters correspond to the fresh gases. Several theoretical curves are also drawn considering the velocity ratio number $V_r(r)$, the vortex power $P(r)$, the Reynolds number $Re(r)$ and the Karlovitz number $Ka(r)$ for the length scale r:

- $V_r(r) = u'(r)/S_L = 1$: A necessary condition for strong interaction (to form a pocket, for instance) is that the velocity induced by the vortex be greater than the laminar burning velocity, that is, $V_r(r) > 1$.
- $P(r) = (r^2 S_L)/(\nu\delta_f) = 1$: By comparing the lifetime of the vortex r^2/ν with the chemical time δ_f/S_L, one can conclude that the vortex will be dissipated before it affects the flame, if $P(r < 1$. $P(r)$ is also a way of quantifying curvature effects: the lower $P(r)$ is, the more important curvature effects are. By using the expression of the flame thickness given in the "Operating Conditions" section and assuming a Prandtl number, Pr, of 0.72, one obtains $P(r) \approx 10(r/\delta_f)^2$. It shifts the line from the position indicated by Poinsot et al. ($r/\delta_f = 1$), but their conclusions about the inability of Kolmogorov scales to alter the flame front remain because the line of the Kolmogorov scales is also shifted ($Re \approx (10u'r)/(S_L\delta_f) = 1$). This is also confirmed by our measurements. As we are only interested in orders of magnitude, we keep the convention of previous studies, though these boundaries might not be perfectly adequate.
- $Re(r) = [u'(r)r]/\nu = 1$: It corresponds to the Kolmogorov scales. If $Re(r) < 1$, then the vortex will be dissipated by viscous effects.
- $Ka(r) = [u'(r)\delta_f]/(rS_L) \approx Re^{-1/2}(\delta_f/\eta)^2 = 1$: This means that a necessary condition to quench the flame front by stretching is $Ka(r) > 1$.

Fig. 3 indicates that the theoretical curves previously described and our experimental results are consistent. Our no-effect limit is much more restrictive than $Re = 1$; that is, vortices must be about 10 times stronger in terms of velocity than the Kolmogorov scales to affect the flame front. There might be a discontinuity between our limit and the one determined in Ref. [6]. This is difficult to prove as investigated regions do not overlap, but it may be due to differences in the configuration (level of heat losses, flame strained or not, etc.). Another problem is the definition of *no-effect* interaction. Driscoll and coworkers used a criterion based on the lengthening of the flame front (5% of length increase), whereas we use a somewhat different criterion (when the height of the flame deformation reaches the characteristic vortex lengthscale r). Comparisons with simulations of Poinsot et al. show a good agreement for $r/\delta_f > 1$, hence supporting the relevance of their conclusions. Nevertheless, our measurements prove that vortices can affect the reactive layer, even if $r/\delta_f < 1$ is contrary to the numerical calculations. Using the expression of the flame thickness shows that the line $P(r) = 1$ is rather located at $r/\delta_f \approx 0.3$ as shown in previous section. Thus, our results do not contradict previous dimensional considerations.

Concerning the wrinkled flame and the pocket formation regimes, the agreement between experimental and numerical results is fairly good. It seems that the limit curve between both regimes presents a *grave accent* shape: small vortices need a high velocity to efficiently curve the flame front because of viscous effects, whereas large vortices need a velocity slightly decreasing with vortex size. For a Lewis

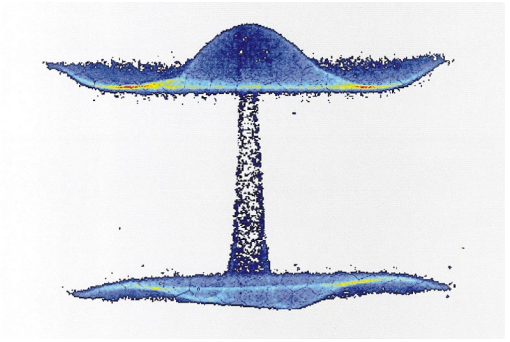

FIG. 4. Double flame/vortex interaction (CH spontaneous emission, $\phi = 0.9$, $Re = 1100$, $u_\theta/S_L = 36.6$, $d/\delta_f = 5.28$).

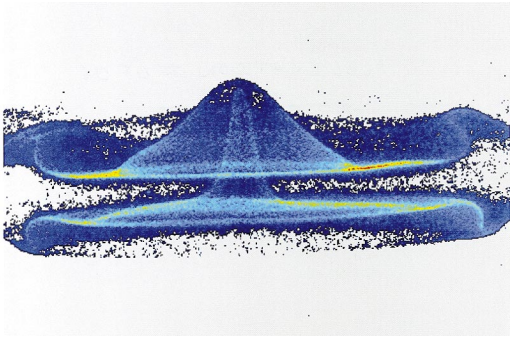

FIG. 5. Double flame/vortex interaction (OH spontaneous emission, $\phi = 0.5$, $Re = 440$, $u_\theta/S_L = 32.4$, $d/\delta_f = 0.83$).

number greater than 1, thermodiffusion effects are stabilizing. They limit the formation of pockets by increasing the flame speed where the flame front is convex with respect to the fresh gases. Our experimental results show that the formation of fresh gas pockets is more difficult when the vortex characteristic size is increased, because of thermodiffusive effects and viscous dissipation that confirms the predictions of Poinsot et al.

Double Premixed Flame/Vortex Interactions

When the vortex crosses the first flame front, it stretches it and pulls it to the second flame front. It is then possible to investigate double premixed flame/vortex interaction. Two configurations are possible: the first one is the case of two flame fronts separated by fresh gases [18], the second one is the case of hot gases between two reactive layers. Our experimental setup only allows the investigation of the second configuration. Depending on the flowrate, it is possible to investigate two limit cases: the first one with the flames very close to each other, the second one with a thick layer of burnt gases.

Figure 4 shows a visualization of CH spontaneous emission ($\phi = 0.9$, $Re = 1100$, $u_\theta/S_L = 36.6$, $d/\delta_f = 5.28$). The distance between both reactive layers is about 57 times the flame thickness. It is unclear in this image whether the lower flame front merged with the upper one. Nevertheless, it is interesting to notice that the first flame front is distorted in a small area with the formation of a cylindrical reactive layer, whereas the second one forms a wide dome. It is not easy to quantify the modifications sustained by the vortex in hot gases. Indeed, the large increase of the kinematic viscosity in burnt gases (typically, a factor of 10) implies a large decrease of the vortex circulation. Thus, the toroidal vortex moves and rotates slower, the ring diameter and the core diameter increase, and in the case studied, the instabilities present in the vortex at the beginning of the interaction with the first flame disappeared. A time ratio $Tr(r) = (r^2u')/(\nu d_f)$ comparing the viscous effects time r^2/ν to the burnt gases crossing time $d_f/U_T \approx d_f/u'$ may be introduced where d_f is the distance between both flames. A necessary criterion for the second flame to be disturbed is therefore $Tr(r) > 1$ (here, $Tr(r) = 10, 1$).

To have an idea of mechanisms occurring in double premixed flame interaction and to check the probability of mutual annihilation, Fig. 5 is an OH spontaneous image of the case of two flames close to each other ($\phi = 0.5$, $Re = 440$, $u_\theta/S_L = 32.4$, $d/\delta_f = 0.83$). The flame fronts are about 2.1 times the flame thickness far from each other. The main features are the same as the previous situation: the vortex collides with the first flame, stretches it in the burnt gas area, and pushes away the second flame front ($Tr(r) = 16.6$). As the second reactive layer is very close to the first one, one can expect that both fronts merge. The experiments performed never exhibit such a process. The reasons might be the following:

- Thermodiffusive effects are stabilizing. The curvature of the first flame front being higher, the change of laminar burning velocity will be higher in it than in the second one. Consequently, it tends to move away from the second flame front. This is all the more important as the vortex is small.
- The flame fronts never stop producing burnt gases in front of each other. It prevents both reactive layers from being in direct contact. Thus, a necessary condition for the two flame fronts to combine is that the vortex time be smaller than the chemical time, that is, $Ka(r) = [u'(r)\delta_f]/(S_L r) > 1$. It can be noticed that this criterion is the same as the quenching one: the mechanisms of quenching and merging compete with each other.

The two cases described early meet this condition:

$Ka(r) = 6.9$ for case 1, $Ka(r) = 39$ for case 2. This indicates that $Ka(r) > 1$ is not sufficient. Other phenomena must be taken into account: a small vortex will be more efficient than a larger vortex with the same Karlovitz number; merging is most likely to occur if both flames exhibit a hole, allowing edges of both to combine.

Summary and Conclusions

Novel experimental results concerning a double premixed flame interacting with a vortex ring are reported. Experiments are conducted on a counterflow burner whereby two flows of air and propane mixture impinge on each other. A vortex ring is then generated from a tube installed in the nozzle on the lower side and impinge on one or both flames depending on the vortex strength. Three of the four well-known kinds of premixed flame/vortex interactions are observed. The main features in predictions of Poinsot et al. are confirmed: the role of heat losses in quenching processes, the importance of thermodiffusive effects (connected to the Lewis number), the competing action of curvature and viscosity.

First investigations of the double premixed flame/vortex interactions in this configuration are performed. The inability of the vortex to perturb widely the second flame when located far away from the first one is emphasized. A new characteristic number $Tr(r)$ is introduced to assess the ability of the vortex to reach the second flame ($Tr(r) > 1$). Competition between flame quenching and merging is underlined. The relevance of the quenching criterion ($Ka(r) > 1$) to partially characterize flame merging is also showed. Further investigations are in progress.

Acknowledgments

We wish to thank Dr. D. Veynante for very fruitful discussions. The Ph.D. of Mr. P. H. Renard is financially supported by a Direction Générale de l'Armement (DGA) fellowship.

REFERENCES

1. Borghi, R., in *Recent Advances in the Aerospace Sciences,* (C. Bruno & C. Casci, eds.), Plenum Press, New York, 1985, pp. 117–138.
2. Williams, F., *Combustion Theory,* 2nd ed., Addison-Wesley, Reading, MA, 1985.
3. Peters, N., in *Twenty-First Symposium (International) on Combustion,* The Combustion Institute, Pittsburgh, 1986, pp. 1231–1250.
4. Poinsot, T., Veynante, D., and Candel, S., *J. Fluid Mech.* 228:561–606 (1991).
5. Poinsot, T., Candel, S., and Trouvé, A., *Prog. Energy Combust. Sci.* 21:531–576 (1996).
6. Roberts, W. and Driscoll, J., *Combust. Flame* 87:245–256 (1991).
7. Roberts, W., Driscoll, J., Drake, M., and Ratcliffe, J., in *Twenty-Fourth Symposium (International) on Combustion,* The Combustion Institute, Pittsburgh, 1992, pp. 169–176.
8. Roberts, W., Driscoll, J., Drake, M., and Goss, L., *Combust. Flame* 94:58–69 (1993).
9. Driscoll, J., Sutkus, D., Roberts, W., Post, M., and Goss, L., *Combust. Sci. Technol.* 96:213–229 (1994).
10. Mueller, C., Driscoll, J., Sutkus, D., Roberts, W., Drake, M., and Smooke, M., *Combust. Flame* 100:323–331 (1995).
11. Hertzberg, J., Namazian, M., and Talbot, L., *Combust. Sci. Technol.* 38:205–216 (1984).
12. Escudié, D. and Charnay, G., in *Fifth Symposium on Turbulent Shear Flows,* Springer-Verlag, Berlin, 1987, pp. 347–360.
13. Escudié, D., *Prog. Astronaut. Aeronaut.* 113:215–239 (1988).
14. Lee, T.-W., *Combust. Sci. Technol.* 90:211–229 (1993).
15. Lee, J., Lee, T.-W., Nye, D., and Santavicca, D., *Combust. Flame* 95:161–168 (1995).
16. Nye, D., Lee, J., Lee, T.-W., and Santavicca, D., *Combust. Flame* 105:167–179 (1996).
17. Nguyen, Q.-V. and Paul, P., in *Twenty-Sixth Symposium (International) on Combustion,* The Combustion Institute, Pittsburgh, 1996, pp. 357–364.
18. François, I., Larrauri, D., and Escudié, D., *Combust. Flame* 110:14–24 (1997).
19. Rolon, J. C., Aguerre, F., and Candel, S., *Combust. Flame* 100:422–429 (1995).
20. Thévenin, D., Rolon, J. C., Renard, P.-H., Kendrick, D., Veynante, D., and Candel, S., in *Twenty-Sixth Symposium (International) on Combustion,* The Combustion Institute, Pittsburgh, 1996, pp. 1079–1086.
21. Renard, P.-H., Rolon, J. C., Thévenin, D., and Candel, S., *Combust. Flame* in press.
22. Dandy, D. and Vosen, S., *Combust. Sci. Technol.* 82:131–150 (1992).
23. Dyer, M. and Crosley, D., in *International Conference Lasers '84,* STS Press, McLean, VA, 1985, p. 211.
24. Garland, N. and Crosley, D., *Appl. Opt.* 24:4229–4237 (1985).
25. Miller, J. and Bowman, C., *Combust. Sci. Technol.* 15:287–338 (1989).
26. Sennoun, M., Djavdan, E., Darabiha, N., and Rolon, J., in *Laser Applications in Combustion and Combustion Diagnostics,* SPIE-The International Society for Optical Engineering, 1993, vol. 1862, pp. 123–132.
27. Sennoun, M., "Étude Numérique et Expérimentale de Flammes Laminaires Étirées de Prémélange Propane-Air," Ph.D. thesis, École Centrale Paris, France, ECP 1994-25, 1994.
28. Sivashinsky, G., *Acta Astron.* 4:1177–1206 (1977).

29. Durox, D., in *Twenty-Fourth Symposium (International) on Combustion,* The Combustion Institute, Pittsburgh, 1992, pp. 197–204.
30. Wu, C. K. and Law, C. K., in *Twentieth Symposium (International) on Combustion,* The Combustion Institute, Pittsburgh, 1984, pp. 1941–1949.
31. Yamaoka, I. and Tsuji, H., in *Twentieth Symposium (International) on Combustion,* The Combustion Institute, Pittsburgh, 1984, pp. 1883–1892.
32. Yu, G., Law, C., and Wu, C., *Combust. Flame* 63:339–347 (1986).